Available online at www.sciencedirect.com
SCIENCE DIRECT
Catalysis Today 111 (2006) 59–67
CATALYSIS TODAY
www.elsevier.com/locate/cattod

Particle size distributions in heterogeneous catalysts: What do they tell us about the sintering mechanism?

Abhaya K. Datye [a,*], Qing Xu [a], Karl C. Kharas [b], Jon M. McCarty [c]

[a] *Department of Chemical & Nuclear Engineering and Center for Microengineered Materials, University of New Mexico, MSC 01 1120, Albuquerque, NM 87131-0001, USA*
[b] *Delphi Catalyst, Tulsa, OK 74158-0970, USA*
[c] *Catalytica Energy Systems Inc., Mountain View, CA 94043, USA*

Available online 29 November 2005

Abstract

Supported metal catalysts were treated at temperatures up to 900 °C, and sintering times up to 4000 h and the particle size distributions were determined via transmission electron microscopy (TEM), SEM and scanning transmission electron microscope (STEM). Sintering conditions were chosen so that the mechanism of sintering would range from Ostwald ripening to particle migration and coalescence. Previous theoretical models have suggested that a size distribution skewed towards small particles can arise from Ostwald ripening, while a size distribution with a long tail towards large particles can only come from particle migration and coalescence. Some of our experimental measurements were performed under conditions that favor Ostwald ripening, while others were performed under conditions that favor particle migration and coalescence. In every instance, the experimental particle size distributions could be fitted to a log normal distribution, and were always skewed to the right, with a tail towards larger particle diameters. Hence, we conclude that no inference about sintering mechanism can be derived from the particle size distribution.

Keywords: Ostwald ripening; Particle migration and coalescence (PMC); Sintering mechanism; Pt/Al_2O_3; Pd/Al_2O_3

1. Introduction

The growth of metal particles and attendant loss of surface area represent a major route for the deactivation of heterogeneous catalysts. The problem becomes much more severe for catalysts that operate at high temperature, such as those used for catalytic combustion of methane [1], in close-coupled automotive exhaust catalysts [2] as well as for steam reforming of methane [3]. Understanding the mechanism of catalyst sintering could be an important first step in devising strategies to synthesize catalysts having greater durability. Previous work has been directed at investigating the mechanism of sintering via in situ observations of supported catalysts. For example, Stone et al. [4] have reported scanning tunneling microscopy (STM) observations of Pd/TiO_2 that show that sintering is entirely dominated by particle migration and coalescence, even at temperatures up to 500 °C. Likewise, in situ transmission electron microscopy (TEM) by Baker et al. [5] also demonstrated the migration of nanoparticles leading to coalescence. One limitation of these in situ studies is that they are performed on model catalyst systems, with metal loading that is higher than in industrial catalysts. The surfaces of these model catalyst systems are smooth, and often do not possess the same surface chemistry as that of high surface area supports. The thin film geometry further limits the temperature and gas environment these model catalysts can be subjected to. To simulate conditions encountered in automotive exhaust catalysis, or during catalytic combustion, it is necessary to perform sintering at elevated temperature (900 °C) and pressure, which necessitate ex situ observation of conventional supported catalysts. The observable parameters in this case are catalyst reactivity, metal and support surface area as well as particle size distribution. It has been suggested that the particle size distribution in the sintered catalyst may provide clues to the operative mechanism for catalyst sintering [6].

Two limiting mechanisms for catalyst sintering have been proposed: Ostwald ripening (OR) and particle migration and coalescence (PMC). Under OR, it is assumed that the metal

* Corresponding author.
E-mail address: datye@unm.edu (A.K. Datye).

0920-5861/$ – see front matter © 2005 Elsevier B.V. All rights reserved.
doi:10.1016/j.cattod.2005.10.013

particles are immobile and sintering occurs solely due to the migration of atoms or clusters from small particles to the large particles. The driving force for sintering comes from the higher chemical potential of the metal atoms in small particles as a consequence of their radius of curvature. The kinetics of OR are given by the Lifshitz–Slyozov–Wagner (LSW) theory [7] which results in a stationary (self-similar) particle size distribution (PSD) and a growth law where $\bar{d}^n$ increases linearly with time. Here, $\bar{d}$ is the number average diameter. The particle size distribution in the LSW model depends on the nature of the rate-limiting step, but all of the forms share two common features, an asymmetric shape skewed to the left and a cut off in the size distribution at a diameter < twice the mean diameter [8]. Fig. 1(a) shows a typical LSW size distribution from the work of Finsy [7] for the case where surface diffusion is the rate-limiting step. The size distribution for PMC is very different in that it is skewed to the right, as shown in Fig. 1(b). The mechanism for PMC was analyzed by Granqvist and Buhrmann [6] who showed that the particle size distribution corresponds to a log normal distribution function (LNDF). Since the particle size distributions for the OR and PMC mechanisms are so different, it was argued that experimental measurements should allow us to determine sintering mechanism. When they analyzed particle size distributions from a number of growth processes, Granqvist and Buhrmann came to the conclusion that PMC was the prevalent sintering mechanism since the size distributions fit the LNDF [9].

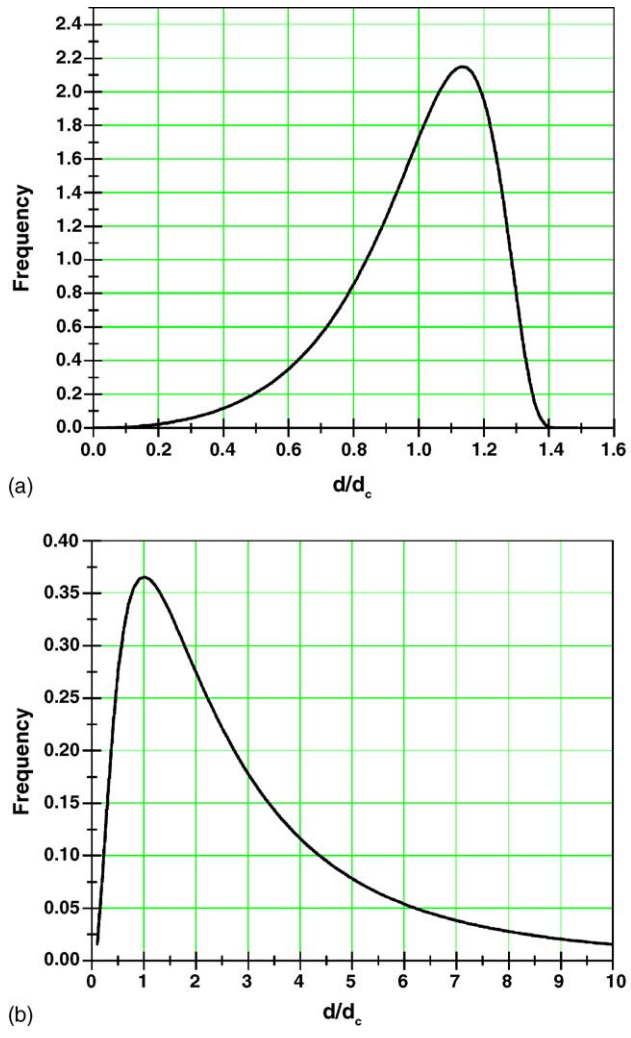

Fig. 1. Calculated particle size distributions for: (a) Ostwald ripening [7] and (b) log normal distribution [6].

The ability to infer mechanism from particle size distributions, and the conclusion that PMC was the sintering mechanism was questioned by Wanke [10], who argued that experimental limitations make it difficult to infer mechanism from PSD's. For instance, if the initial size distribution is log normal, it might take a long time for the PSD to evolve to the LSW model. A second major point of contention by Wanke [10] had to do with the ability to detect small particles (<1.5 nm) by TEM. This resolution limitation of TEM would limit our ability to get accurate size distributions, the uncertainty being greatest when counting the small particles, which is the region where the two distributions differ (see Fig. 1). However, much has changed since Wanke's paper [10] was published, prompting us to do a careful examination of particle size distributions in supported metal catalysts. The first major development is the easy availability of high angle annular dark field (HAADF) imaging in a 200 kV scanning transmission electron microscope (STEM) which provides a probe size less than 0.2 nm, increasing the reliability of detection of heavy metal particles below 1 nm in diameter on light element supports [11]. Scanning tunneling microscopy allows us to achieve atomic resolution [4] so that the smallest particle sizes could, in principle, be measured.

In this study, we have chosen a range of environments so that differing mechanistic regimes can be explored. The particle evolution kinetics for Pd sintering at $T > 900\ ^\circ$C implicate Ostwald ripening as the mechanism of sintering while Pt sintering at 600–700 °C in H_2 appears to represent a case of particle migration and coalescence. However, when we switch to oxidizing conditions, we find a dramatic increase in Pt sintering rate, suggesting a change in mechanism. Therefore, these experimental measurements allow us to explore the connection between sintering mechanism and observed particle size distributions.

2. Experimental

2.1. Catalyst preparation

Two separate series of Pd sintering experiments were carried out. One series at the University of New Mexico (UNM) and the other at Catalytica Energy Systems Inc. (CESI). The Pd catalysts in the UNM study were prepared using SCCa90 alumina supplied by Condea Vista Co. (now Sasolchemie GMBH). SCCa90 alumina consists primarily of the transitional θ (and to a lesser extent δ) phase and has a BET surface area of about 90 m^2/g. All catalysts were prepared by impregnation of an aqueous solution of $Pd(NO_3)_2$ onto the support, followed by drying and calcination at 600 °C in air. The catalysts were ball milled using ZrO_2 media during impregnation. The Pd metal loading in these catalysts was varied over a wide range (0.1–7.0 wt.%) to enable a study of metal loading. For this study, we have considered only the

sintering of 7.0 wt.% Pd/alumina. The results of the complete study are reported elsewhere [12]. Sintering was performed on catalyst powders (not pellets) under isothermal conditions at a temperature of 900 °C in an atmosphere of 10 mol% H_2O in N_2. The 10 mol% H_2O was added to mimic exhaust from any combustion process. For each sintering experiment, the furnace tube was flushed with the sintering gas at 300 standard cubic centimeter per minute (SCCM) for 90 min before the start of the experiment. Next, the oven temperature was ramped up at 3 °C/min with the sintering gas at 50 SCCM until 900 °C was reached. The starting time ($t = 0$ h) was taken as the time when the oven temperature reached 900 °C. After the sample had been sintered for the desired length of time the sample was removed and dropped immediately in liquid nitrogen to quench it and preserve Pd in the metallic state. Sintering was also performed in air to verify the role of atmosphere, but we found no effect since PdO decomposes at 900 °C into metallic Pd. Hence, our results pertain to sintering of metallic Pd.

The 15 wt.% Pd catalyst used in the CESI study was prepared over a 5 wt.% silica-stabilized gamma-alumina support (Davison) by two-step impregnation with an aqueous palladium nitrate solution followed by oven drying at 120 °C and calcination in air to 1000 °C for 10 h. The catalyst powder was aged at 950 °C over a progressive series of periods to 4000 h in a purged 9.5 atm internally heated furnace with 14 vol% O_2, 10 vol% H_2O, 4 vol% CO_2, 0.5 ppmv SO_2 balance N_2. Trace sulphur was introduced by dissolving dimethyl sulfonic oxide in the vaporized water that introduced steam to a 500 mL/min flow of premixed flushing gas containing oxygen, carbon dioxide and nitrogen. The alumina-lined aging furnace was flushed with pure N_2 at the end of the run to avoid reoxidation of the supported Pd metal particles. Powders of several catalysts were placed in alumina trays, which were stacked in the furnace in a silica–alumina tray holder. Further details are provided elsewhere [1].

The 0.5 wt.% Pt/Al_2O_3 catalyst was obtained from Engelhard Corporation. The sintering was performed at atmospheric pressure (630 Torr in Albuquerque) with 7 mol% H_2, 10 mol% H_2O in N_2 and also in 10 mol% H_2O in air to represent reducing and oxidizing conditions, respectively. The H_2 was added in the case of Pt sintering to ensure that we maintained Pt in the metallic state during the sintering process. The sintering temperature was 600 °C and 700 °C with a sintering time of 96 h and the sintering procedure was similar to that described above for Pd sintering at 900 °C.

2.2. Transmission electron microscopy

TEM images were obtained on a JEOL 2010 EX instrument operated at 200 kV with a LaB_6 emitter. This microscope provides a point resolution of 0.19 nm. The imaging of the Pt and 15 wt.% Pd was performed with a JEOL 2010 F microscope having an ultimate resolution of 0.14 nm for STEM high angle annular dark field imaging. For some of the 15 wt.% Pd samples, due to the large particle sizes, we also used a Hitachi S-800 field emission scanning electron microscope. Sample preparation involved grinding the catalyst with a mortar and pestle, suspending it in ethanol and depositing a drop of the suspension on a Cu TEM grid or on an SEM stub. This procedure allowed a very thin layer of the catalyst sample to be deposited on the grid, avoiding overlap between catalyst particles and making it easier to image the metal particles in thin regions of the support. The images were recorded using Digital Micrograph software. Particle size distributions were obtained by counting between 100 and 1000 particles on each sample. The size distributions were fitted to a log normal distribution in each case. From the size distribution, we determined the following averages: the number average diameter $d_n = \sum n_i d_i / \sum n_i$, the surface average diameter $d_s = \sum n_i d_i^3 / \sum n_i d_i^2$ and the volume average diameter $d_v = \sum n_i d_i^4 / \sum n_i d_i^3$, where n_i is the number of particles with diameter d_i.

3. Results and discussion

3.1. Isothermal sintering of Pd

Sintering of Pd at UNM which was carried out at atmospheric pressure (630 Torr in Albuquerque) and an atmosphere of 10% H_2O in flowing N_2 at 900 °C [12]. The second series of sintering experiments at CESI [1] were also conducted at 950 °C but at 9.5 atm in a flowing N_2 stream containing 14 vol% O_2, 10 vol% H_2O, 4 vol% CO_2, 0.5 ppmv SO_2. Particle sizes were measured using a TEM for the 7 wt.% Pd sample and a combination of TEM and SEM for the 15 wt.% Pd sample since the particle sizes extend all the way to the micron regime in this case. The sintering kinetics in both of these studies were similar and could be fitted to a model of the type $d^n - d_0^n = kt$, where d is the mean diameter at time t and d_0 is the mean diameter at the start of the experiment ($t = 0$). The major difference between these two studies was that the exponent n was approximately 2 for the UNM data, while the exponent was 3 in the CESI study. The results of the longer term study, spanning 4000 h of sintering, are reproduced here in Fig. 2 from McCarty et al. [1]. We see from Fig. 2 that Pd dispersion continues to decrease with time, following an nth

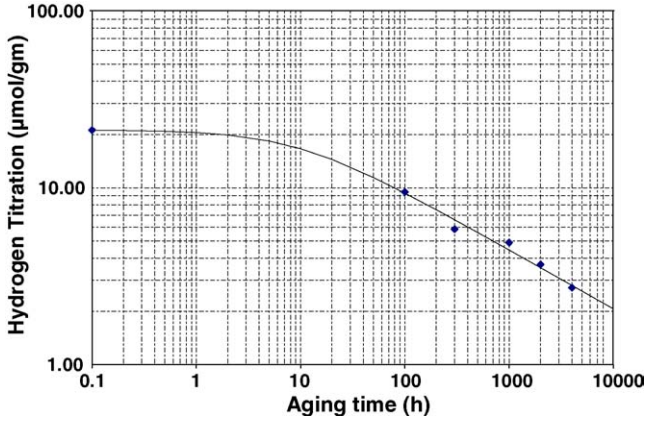

Fig. 2. Sintering of 15 wt.% Pd/silica–alumina at 950 °C, plotted in terms of exposed Pd content (H_2 titration value—S) as function of time and fitted to the function $S^{-3} - (S_0)^{-3} = kt$. S_0 is the initial uptake at time 0, reported here as 0.1 h (reproduced/adapted with permission from ref. [1], copyright 2005 American Chemical Society).

order power law. There is no limiting, or equilibrium dispersion at this sintering temperature. Such behavior is not consistent with particle migration and coalescence since the rates of particle migration would be expected to slow down with increase in particle size. *n*th order kinetics are consistent with the LSW model for sintering [8], and would imply that Ostwald ripening is the prevalent mechanism for Pd sintering at these temperatures. Pd has a vapor pressure of 6.8×10^{-8} Torr at 900 °C [13], and in vacuum we would expect to lose a monolayer of Pd atoms every 20 s. Control experiments on a model catalyst have verified such a loss of Pd metal [14]. There is therefore a high likelihood that Pd atoms can be emitted from the particle surface. On the other hand, at the higher total pressure used in the CESI study and in the presence of oxygen, the volatilization of Pd may be suppressed. We suggest that the differing exponents ($n = 2$ and 3) in these two sintering studies may be the result of a shift in mechanism from vapor phase diffusion to surface diffusion over the support.

Fig. 3 shows the particle size distributions from both of these sintering studies. The smooth curves represent a fit to the log normal distribution function. The data are presented in terms of frequency (%) as a function of particle size. These curves are not normalized in any way, and the variations in peak height have no significance. The peak maxima change only because the bin size was adjusted as particle size increased. The important conclusion from this figure is that as the mean particle size increases from 20 nm all the way to 500 nm, the size distributions remain self-similar and follow the LNDF model. Also, the smallest detected particle size keeps increasing with sintering time. Tables 1 and 2 provide further details on the particle size distributions showing only a modest increase from 1.24 to 1.53 for the standard deviation with increasing sintering time. These particle size distributions are not consistent with the classical LSW model, which would predict a distribution skewed towards smaller diameters. The mechanism of Ostwald ripening implies that small particles shrink in size as atoms are transported to larger particles. Hence, smaller particles should continually be generated as sintering proceeds. Table 1 shows, however, that the smallest detectable particle keeps increasing in size with sintering time. The inability to detect smaller particles with increased sintering time cannot be due to limitations in instrumental resolution, which in our case is well under 1 nm. A similar inability to detect smaller particles was noted in the STM study of Pd sintering by Stone et al. [4]. We will discuss this apparent discrepancy in a later section of this manuscript. Next, we describe the sintering of Pt, which at 700 °C has an estimated vapor pressure of 1×10^{-20} Torr [15]. The low vapor pressure for Pt should slow down the rate of Ostwald ripening and allow us to study other mechanistic regimes.

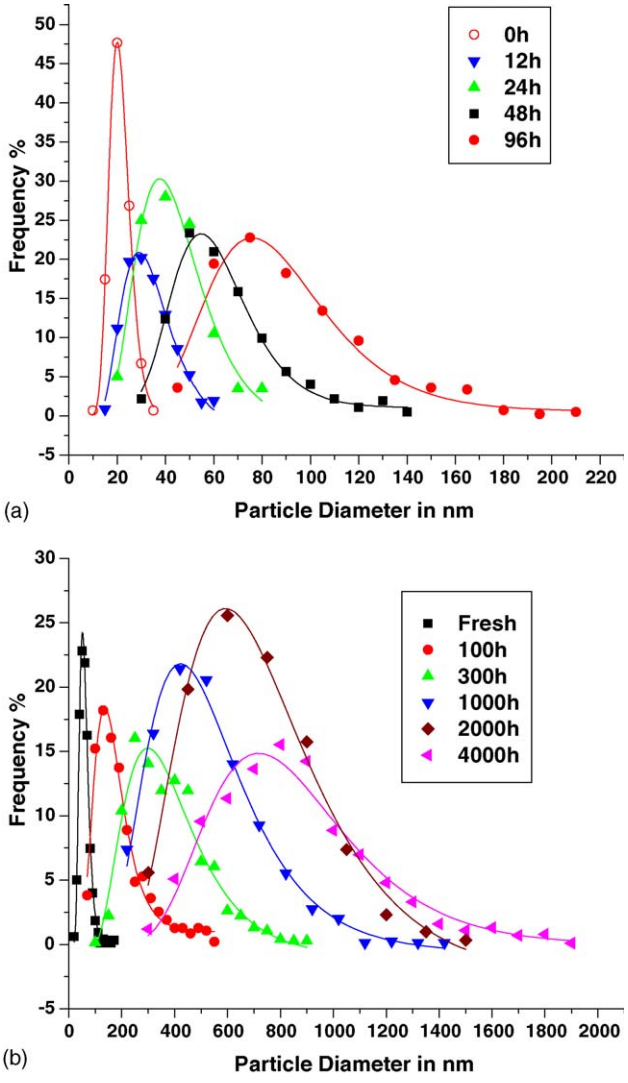

Fig. 3. Particle size distributions after sintering at 900 °C for differing lengths of time. All data have been fitted using a log normal distribution: (a) 7 wt.% Pd/alumina and (b) 15 wt.% Pd/silica–alumina.

Table 1
Particle size distributions for the 7 wt.% Pd/SCCa—UNM study

Sintering time (h)	Number of particles counted	Number average (nm)	Standard deviation (σ)	Smallest particle size detected, d (nm)	Largest particle size detected, d (nm)
0	149	17.8	1.24	9.2	33.9
6	235	24.8	1.35	12.7	59.4
12	463	30.1	1.37	15.2	71.5
24	200	35.8	1.42	16.1	79.6
48	372	57.5	1.41	22.2	136.0
96	420	81.4	1.44	36.5	298.2

Table 2
Particle size distributions for the 15 wt.% Pd/silica–alumina—Catalytica study

Sintering time (h)	Number of particles counted	Number average (nm)	Standard deviation (σ)	Smallest particle size detected, d (nm)	Largest particle size detected, d (nm)
0	979	54.1	1.36	10.2	169.1[a]
100	461	171.3	1.46	42.5	582.5
300	757	349.6	1.50	100	1100
1000	789	467.1	1.53	140	1400
2000	609	621.5	1.55	160	1400
4000	975	773.0	1.43	230	1830

[a] The fresh catalyst had a few particles >170 nm ranging all the way up to 1400 nm, however due to inadequate statistics we have cut off the distribution at 169.1 nm.

3.2. Isothermal sintering of Pt

Figs. 4–6 show STEM images of the Pt catalyst in its fresh state and after various sintering treatments. The particle size distributions were fitted to the LNDF model and the mean diameter and standard deviation are listed in the figure. For the LNDF model, the mean diameter represents the geometric mean. We have also computed the number average, or arithmetic mean, which is reported in Table 3. As seen in Figs. 5 and 6 and Table 3, the effect of atmosphere on sintering rate is striking. Sintering in a reducing atmosphere at 600 °C and 700 °C caused only a modest increase in average particle diameter from 2.4 nm to 3.5 nm and 4.5 nm, respectively. As we expected, Ostwald ripening of Pt should be extremely slow at this temperature. However, treating in air at the same temperature increased the average particle diameter dramatically, to 14.6 nm and 31.1 nm, respectively. A plausible reason for the increased sintering in air could be that the presence of residual chloride from the chloroplatinic acid precursor in presence of air leads to volatile species that enhance sintering rate. Treatment of spent reforming catalysts in air in the presence of chlorine is known to help redispersion [16]. We would like to determine if it is chlorine or oxygen that is responsible. Since treatment in H_2 can remove chloride from a supported alumina catalyst, we treated these Pt catalysts in H_2 for 96 h at 600 °C and 700 °C prior to the sintering treatment to eliminate any possible influence of residual chloride. As shown in Table 4, the extent of sintering in air was identical with and without the hydrogen pretreatment. We therefore conclude that sintering in air proceeds much faster than sintering in H_2.

Our results on Pt sintering are consistent with other observations in the literature. The study by Smith et al. [17] showed that the mean particle diameter of a Pt/Al_2O_3 catalyst increased from 1.8 nm to 43.0 nm when treated in N_2 containing 3% by volume of O_2 at 600 °C for 2 h, while a similar treatment in pure H_2 only produced an increase in mean diameter to 4.1 nm. The effect of oxygen in promoting sintering has also been reported in the review paper by Wynblatt and Gjostein [8]. It is well known that the oxide of platinum is volatile and could lead to enhanced interparticle transport. On flat model catalysts, Wynblatt and Gjostein [8] report a loss of Pt due to evaporation when treated in air. A volatile platinum oxide, PtO_2, was proposed to form through the following reaction:

$$Pt(s) + O_2(g) = PtO_2(g)$$

The enthalpy change for this reaction is ~175 kJ/mol, which is considerably smaller than either the sublimation energy for platinum (~565 kJ/mol), or the energy required to transfer Pt atoms from a particle to the substrate (527 kJ/mol) [18]. Thus, in an oxidizing atmosphere the escape of Pt from a particle in the form of PtO_2 is much more favorable thermodynamically than the escape of Pt atoms [18]. Ostwald ripening may therefore occur through the migration of PtO_2 in the vapor phase or

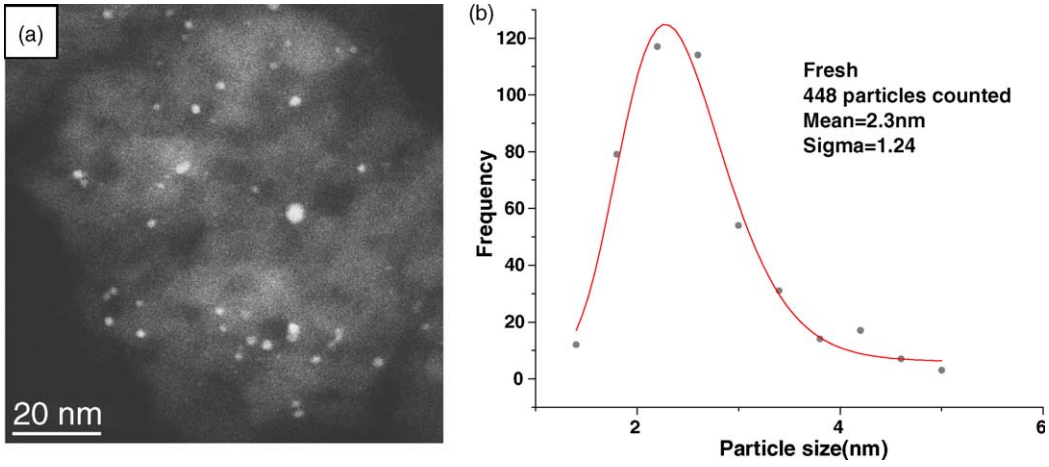

Fig. 4. STEM image (a) and particle size distribution (b) of fresh 0.5% Pt/Al_2O_3. The line shows a fit to the log normal distribution function.

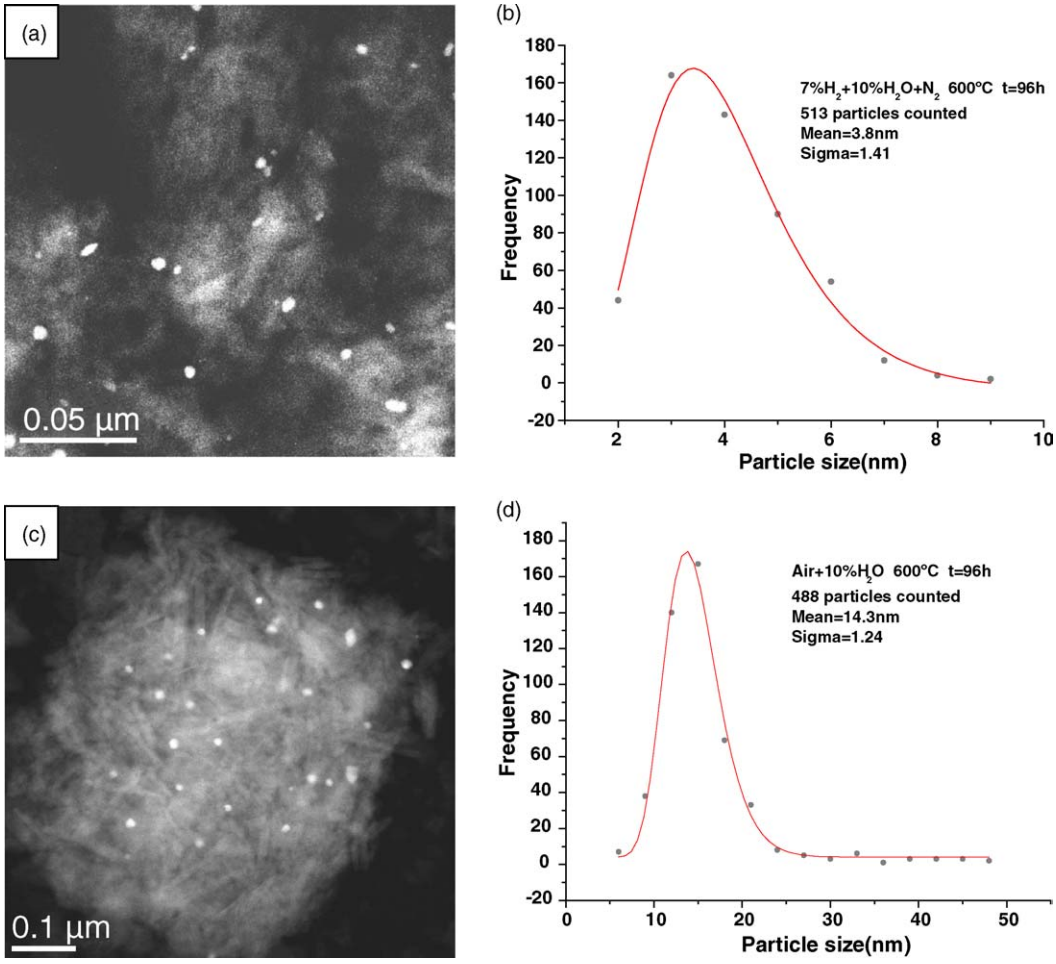

Fig. 5. STEM images (left) and PSDs (right) of 0.5% Pt/Al_2O_3 treated at 600 °C in 7% H_2 + 10% H_2O in N_2 for 96 h (a and b) and in 10% H_2O in air for 96 h (c and d). The lines show fits to the LNDF.

through the migration of adsorbed PtO_2 over the support. After the sample is cooled and observed in the TEM, we detect only metallic Pt particles indicating that PtO_2 is not thermodynamically stable. We infer that the PtO_2 must be a transient species that assists the sintering process in air.

In a H_2 atmosphere, we would expect that the low vapor pressure of metallic Pt at 700 °C (estimated vapor pressure of 1×10^{-20} Torr [15]) would cause the rate of Ostwald ripening to be negligible. Since the Pt particle sizes are very small (<5 nm), and Pt has been shown to be mobile at these temperatures, it is reasonable to assume that growth occurs via particle migration and coalescence. Therefore, we propose that the change in sintering atmosphere leads to a shift in sintering mechanism, from particle migration and coalescence (under reducing conditions) to Ostwald ripening (sintering in air). Since molecular species such as PtO_2 have a much higher diffusivity than metal particles, we can explain the enhanced rate of sintering of Pt in air compared to H_2. We can now examine the particle size distributions in light of this shift in mechanism. As seen in Figs. 5 and 6, the particle size distributions for Pt sintered in H_2 or in air can both be easily fitted to the LNDF model. It appears that despite a shift in sintering mechanism, evident from a dramatically different rate of sintering, there is no effect on the experimentally measured particle size distribution.

3.3. Relationship between sintering mechanism and particle size distribution

A number of studies in the literature have attempted to make a connection between the particle size distribution and sintering mechanism. One of the earliest studies was by Granqvist and Buhrmann [6] who scrutinized a number of published size distributions and advocated the view that coalescence growth provided the most plausible explanation for sintering mechanism. Their argument was based on the fact that their theoretical development provided a rigorous justification for migration and coalescence mechanism leading to a log normal size distribution. Indeed, examining the literature on experimentally observed particle size distribution, we see most studies reporting a good fit to the LNDF model [19,20]. The work presented here is no exception, with all of our data fitting the LNDF model as well. On the other hand, most published theoretical size distributions for the LSW model predict a distribution skewed towards the smaller particle sizes [8,21,22].

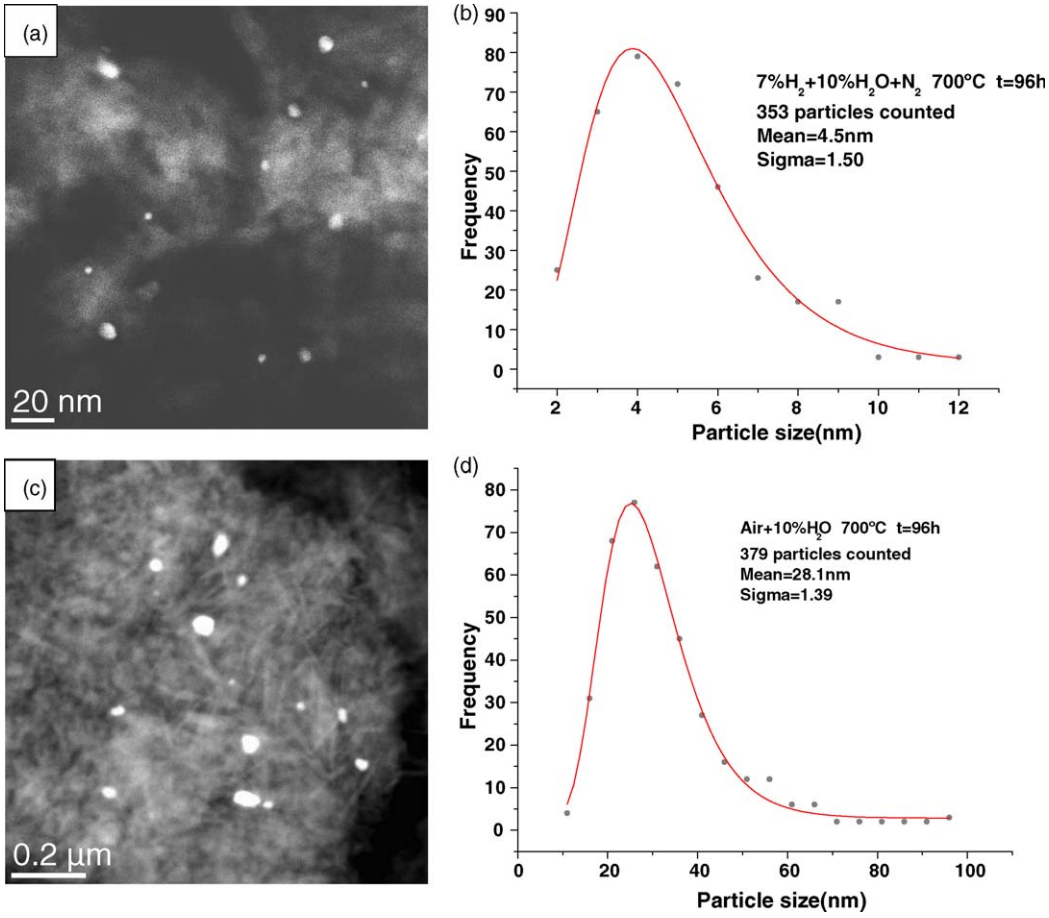

Fig. 6. STEM images (left) and PSDs (right) of 0.5% Pt/Al_2O_3 treated at 700 °C in 7% H_2 + 10% H_2O in N_2 for 96 h (a and b) and in 10% H_2O in air for 96 h (c and d). The lines show fits to the LNDF.

We embarked on this study with the thinking that improved detection of small particles using the HAADF imaging mode should allow us to see if smaller particles are being generated due to Ostwald ripening. Our experiments on Pd were performed under conditions where we can be confident that sintering occurs via Ostwald ripening. In the case of Pt sintering in air, we again feel comfortable in concluding that sintering in air is dominated by transport of volatile platinum oxide species, hence an Ostwald ripening process. However, in both cases we fail to detect any smaller particles being generated with increasing sintering time. It appears that any small particles that are being generated due to the ripening process are disappearing faster than they are being created, so we do not see them experimentally. A key assumption in the theoretical treatments of Ostwald ripening is that the particles are immobile, but there is plenty of evidence that small particles can migrate and coalesce. Hence, if particle migration and coalescence occurs simultaneously with ripening, we may lose any small particles that are created. Another possibility is that there is an error in the derivation of the LSW model as applied to sintering on nano-sized metal particles on a surface. This was the argument made by Jak et al. [23] in their study of Pd sintering on TiO_2(1 1 0). They questioned the assumption made in all derivations of the LSW model that the exponential term in the Gibbs Thompson equation can be linearized to yield a mathematically simpler form for the surface concentration of adatoms. The expansion of the exponential term is not justified in the case of very small particles, such as the 1 nm Pd particles

Table 3
Effect of atmosphere on mean particle diameter of 0.5% Pt/Al_2O_3 sintered at 600 °C and 700 °C for 96 h

Sample treatment	Number average diameter (nm)	Standard deviation (σ)
Fresh	2.4	1.24
7% H_2 + 10% H_2O in N_2 600 °C	3.5	1.41
10% H_2O in air 600 °C	14.6	1.24
7% H_2 + 10% H_2O in N_2 700 °C	4.5	1.50
10% H_2O in air 700 °C	31.1	1.39

Table 4
Results of 96 h treatment in flowing H_2 on sintering of 0.5 wt.% Pt/Al_2O_3 air

Temperature (°C)	Treatment	Average diameter (nm)
600	96 h in air	14.6
	96 h in H_2, then 96 h in air	15.5
700	96 h in air	31.1
	96 h in H_2, then 96 h in air	34.4

studied by Jak et al. [23]. If the exponential term is retained, and the resulting non linear equations are integrated numerically, even the Ostwald ripening model yields a size distribution without a pronounced tail on the small diameter side. Therefore, according to Jak et al. [23], the absence of small particles in the particle size distribution cannot be used to rule out Ostwald ripening as the prevailing mechanism. Another assumption that breaks down when dealing with nano-sized particles is that of constant surface tension. Campbell et al. [24] derived a theoretical formulation for the variation in surface tension with size, and were able to obtain better agreement with observed sintering rate.

In the Pd study reported here, the smallest particle size detected starts out around 20 nm, where the linearization of the Gibbs equation may be justified and one would not expect any influence of the particle size on surface tension. In this size regime, we cannot invoke the explanation proposed by Jak et al. [23] to explain the discrepancy between the LSW model and the experimentally observed particle size distribution. We also need to address the long tail in experimentally observed size distributions on the large diameter side, a feature not seen in the classical LSW model which predicts a cut off at 1.33–2 times the mean diameter. Our experimental data in Table 1 show no such upper bound on the particle sizes in the sintered catalysts. This discrepancy has prompted a number of authors to suggest modifications to the classic LSW model [25–27] which predicts a unique size distribution for each rate-limiting condition. Fuentes and Salinas-Rodriguez [27] relaxed one of the constraints in the derivation, allowing them to propose a number of possible size distributions. In this manner, they were able to find modified LSW size distributions that matched the LNDF model with very little error. Their work implies that sintering could occur via OR or PMC and we can still end up with a size distributions that follows the LNDF model. Our experimental work is in agreement with this hypothesis, since we find all of our measured size distributions fit the LNDF model, regardless of the mean size or sintering conditions.

4. Conclusions

This study has presented particle size distributions for the sintering of metallic Pd at 900 °C and 950 °C and for the sintering of Pt under reducing and oxidizing conditions at 600 °C and 700 °C. Sintering was performed for ∼100 h in all cases, except in the case of a 15 wt.% Pd catalyst where the sintering was continued further up to 4000 h. Based on the available evidence, we conclude that the sintering of Pd at $T > 900$ °C occurs via interparticle transport due to the high vapor pressure of Pd at this temperature. The growth laws for Pd particle evolution were also consistent with the Ostwald ripening mechanism. The low vapor pressure of metallic Pt at 700 °C would cause the rate of Ostwald ripening to be negligible. Since the Pt particle sizes are very small (<5 nm) and small particles are known to be mobile [19,23], it is reasonable to assume that growth occurs via particle migration and coalescence. However, sintering of Pt in air was much faster at these same temperatures, due to formation of a volatile oxide which can enhance interparticle transport. We infer that the dramatic increase in sintering rate in air is a result of a shift in mechanism from particle migration to Ostwald ripening. Therefore, our experimental measurements of particle size distributions represent sintering under Ostwald ripening as well as particle migration and coalescence. All of our measured size distributions could be fit the log normal distribution function, with a long tail extending to large diameters.

We can now assess the validity of the heuristics that are commonly used to infer sintering mechanism from particle size distributions. The classical development of the LSW model for Ostwald ripening leads to a size distribution skewed towards smaller particles, as shown in Fig. 1(a). In the literature, we find only a few instances where classical LSW-type size distributions were reported experimentally. Zinke-Allmang et al. [28] found very good agreement with the LSW model during the growth of Ge on Si(1 0 0). Rosenfeld et al. [29] also report left-skewed size distributions in their work on Ag islands deposited on Ag(1 1 1) but they point out that the mean field approximation implicit in the LSW model leads to narrower distributions than the one they observe experimentally. If we turn to supported metal catalysts, none of the reported studies, including ours, show a size distribution with a tail towards small diameters. Likewise, the evolution of droplet size distribution of a tetradecane emulsion in water [30], while following LSW kinetics for growth of droplet size, shows a more symmetrical size distribution than that predicted by the LSW model. We therefore conclude that a left-skewed distribution is not seen in most studies because small particles generated via ripening may be swept away, either via migration and coalescence, or these small particles are inherently unstable as suggested by Jak et al. [23]. We propose therefore that the absence of a pronounced tail towards small particles in a size distribution should not be used as a criterion for ruling out Ostwald ripening as the prevailing mechanism.

A second heuristic commonly used for inferring mechanism is that right-skewed size distributions, with a long tail towards larger particle diameters, must be a result of particle migration and coalescence. One justification for this heuristic is that the classical LSW model predicts a cut off in the particle size distribution at particle sizes equal to 1.33, 1.5 or 2 times the mean diameter, depending on the rate-limiting step [8]. Most experimental measurements do not show such a well-defined cut off. Since modified LSW models [25–27] have been proposed that result in size distributions skewed to the right, very similar to the LNDF model, we conclude that a right-skewed size distribution cannot be used to rule out Ostwald ripening as a growth mechanism.

Our experimental measurements also show a long tail in the size distribution, extending to extremely large particles. In a catalyst with high metal loading, poor distribution of the metal precursor may cause a long tail towards large particles, which could then persist throughout the entire sintering study. This is possible in the case of the 15 wt.% Pd catalyst we studied, where we found a few particles as large as 1.4 μm even in the fresh catalyst. On the other hand, with the 7 wt.% Pd and the 0.5 wt.% Pt catalysts, no such tail was seen in the fresh catalyst.

After sintering we do see the presence of particles several times the mean diameter. While it is difficult to obtain reliable statistics for these larger particles since they are so few in number, they do consume a significant amount of the precious metal. Hence, it is important to understand the physical processes that lead to this tail in the size distribution. Classical simulations of Ostwald ripening do not show any particles exceeding twice the mean diameter. The modified size distributions proposed recently do allow for a right-skewed distribution, but the existence of such a long tail towards large particles cannot be fully explained at present with the current models for catalyst sintering and therefore deserves further study.

Acknowledgements

This paper was presented at a special symposium organized by Haldor Topsoe A/S at Havreholm, Denmark, in February 2005, in honor of Dr. Jens Rostrup Neilsen and Dr. Henrik Topsoe. The authors would like to congratulate both Jens and Henrik for their inspiring work in the field of heterogeneous catalysis. This author (AD) thanks both of them for their encouragement to pursue fundamental studies of catalyst sintering, and for the collaboration with scientists at HTAS which were initiated during a sabbatical visit to Denmark in 1999. Financial support for this study was provided by the US National Science Foundation, GOALI program, grant CTS-99-11174 and from Delphi Catalysts, Tulsa, OK. The electron microscopy was performed at the microscopy facility in the Earth and Planetary Sciences Department at UNM using a FEG TEM acquired via NSF grant CTS 98-71292.

References

[1] J.G. McCarty, G. Malukhin, D.M. Poojary, A.K. Datye, Q. Xu, Thermal coarsening of supported palladium combustion catalysts, J. Phys. Chem. B 109 (2005) 2387–2391.
[2] S.J. Myers, D.J. Ball, S.M. Ciosek, J.M. Doud, J.C. Schaffer, A.G. Turek, Advancements in Converter Durability to Enable Close Mounted Converters for Stringent Emissions Regulations, Society of Automotive Engineers, 1999, pp. 20–28 (Special Publication SP, SP-1478).
[3] J.R. Rostrup Nielsen, Industrial catalysis; the science and the challenge: conversion of fossil-fuels, Catal. Today 18 (1993) 125–145.
[4] P. Stone, S. Poulston, R.A. Bennett, M. Bowker, Scanning tunneling microscopy investigation of sintering in a model supported catalyst: nanoscale Pd on TiO_2(1 1 0), Chem. Commun. (1998) 1369–1370.
[5] R.T.K. Baker, P.S. Harris, R.B. Thomas, Direct observation of particle mobility on a surface in a gaseous environment, Surf. Sci. 46 (1974) 311.
[6] C.G. Granqvist, R.A. Buhrman, Size distributions for supported metal catalysts: coalescence growth versus Ostwald ripening, J. Catal. 42 (1976) 477.
[7] R. Finsy, On the critical radius in Ostwald ripening, Langmuir 20 (2004) 2975–2976.
[8] P. Wynblatt, N.A. Gjostein, Supported metal crystallites, Prog. Solid State Chem. 9 (1975) 21.
[9] C.G. Granqvist, R.A. Buhrman, Ultrafine metal particles, J. Appl. Phys. 47 (1976) 2200–2219.
[10] S.E. Wanke, Comments on the sintering mechanism of supported metal catalysts, J. Catal. 46 (1977) 234–237.
[11] M.T. Bore, H.N. Pham, E.E. Switzer, T.L. Ward, A. Fukuoka, A.K. Datye, The role of pore size and structure on the thermal stability of gold nanoparticles within mesoporous silica, J. Phys. Chem. B 109 (2005) 2873–2880.
[12] Q. Xu, The sintering of supported Pd automotive catalysts, Ph.D. Thesis, University of New Mexico, Department of Chemistry, 2002.
[13] R. Glang, Vacuum evaporation, in: L. Maissel, R. Glang (Eds.), Handbook of Thin Film Technology, McGraw-Hill Inc., 1970.
[14] R. Goeke, Model supports for studies of catalyst sintering, M.S. Thesis, University of New Mexico, Department of Chemical & Nuclear Engineering, 2003.
[15] J.W. Arblaster, The thermodynamic properties of platinum, Platinum Met. Rev. 49 (2005) 141–149.
[16] S.C. Fung, S.J. Tauster, J.Y. Koo, Method of regenerating a deactivated catalyst, USA Patent 4,925,819 (May 15, 1990).
[17] D.J. Smith, D. White, T. Baird, J.R. Fryer, The characterization of a model platinum/alumina catalyst by high-resolution electron microscopy, J. Catal. 81 (1983) 107–118.
[18] P.J.F. Harris, Growth and structure of supported metal catalyst particles, Int. Mater. Rev. 40 (1995) 97–115.
[19] J.T. Richardson, J.G. Crump, Crystallite size distributions of sintered nickel catalysts, J. Catal. 57 (1979) 417–425.
[20] J. Sehested, A. Carlsson, T. Janssens, P. Hansen, A. Datye, Sintering of nickel steam-reforming catalysts on $MgAl_2O_4$ spinel supports, J. Catal. 197 (2001) 200–209.
[21] B.K. Chakraverty, Grain size distribution in thin films—1. Conservative systems, J. Phys. Chem. Solids 28 (1967) 2401–2412.
[22] M. Agnelli, M. Kolb, C. Mirodatos, Co hydrogenation on a nickel-catalyst. 1. Kinetics and modeling of a low-temperature sintering process, J. Catal. 148 (1994) 9–21.
[23] M.J.J. Jak, C. Konstapel, A. van Kreuningen, J. Verhoeven, J.W.M. Frenken, Scanning tunnelling microscopy study of the growth of small palladium particles on TiO_2(1 1 0), Surf. Sci. 457 (2000) 295–310.
[24] C.T. Campbell, S.C. Parker, D.E. Starr, The effect of size-dependent nanoparticle energetics on catalyst sintering, Science (Washington, DC, USA) 298 (2002) 811–814.
[25] L.C. Brown, A new examination of classical coarsening theory, Acta Metall. 37 (1989) 71–77.
[26] S.D. Coughlan, M.A. Fortes, Self-similar size distributions in particle coarsening, Scripta Metall. Mater. 28 (1993) 1471–1476.
[27] G.A. Fuentes, E. Salinas-Rodriguez, Realistic particle size distributions during sintering by Ostwald ripening, Studies Surf. Sci. Catal. 139 (2001) 503–510.
[28] M. Zinke-Allmang, L.C. Feldman, S. Nakahara, B.A. Davidson, Growth mechanism and clustering phenomena, Phys. Rev. B 39 (1989) 7848–7851.
[29] G. Rosenfeld, K. Morgenstern, M. Esser, G. Comsa, Dynamics and stability of nanostructures on metal surfaces, Appl. Phys. A: Mater. Sci. Process. 69 (1999) 489–496.
[30] Y. De Smet, D. Danino, L. Deriemaeker, Y. Talmon, R. Finsy, Ostwald ripening in the transient regime: a Cryo-TEM study, Langmuir 16 (2000) 961–967.